Multi-modal anatomical Optical Coherence Tomography and CT for *in vivo* Dynamic Upper Airway Imaging

Santosh Balakrishnan[a], Ruofei Bu[a], Hillel Price[b], Carlton Zdanski[d], Amy L. Oldenburg[a,b,c]

[a]Department of Biomedical Engineering, University of North Carolina at Chapel Hill; [b]Department of Physics and Astronomy, University of North Carolina at Chapel Hill; [c]Biomedical Research Imaging Center, University of North Carolina at Chapel Hill; [d]Department of Otolaryngology/Head and Neck Surgery, University of North Carolina at Chapel Hill

ABSTRACT

We describe a novel, multi-modal imaging protocol for validating quantitative dynamic airway imaging performed using anatomical Optical Coherence Tomography (aOCT). The aOCT system consists of a catheter-based aOCT probe that is deployed via a bronchoscope, while a programmable ventilator is used to control airway pressure. This setup is employed on the bed of a Siemens Biograph CT system capable of performing respiratory-gated acquisitions. In this arrangement the position of the aOCT catheter may be visualized with CT to aid in co-registration. Utilizing this setup we investigate multiple respiratory pressure parameters with aOCT, and respiratory-gated CT, on both *ex vivo* porcine trachea and live, anesthetized pigs. This acquisition protocol has enabled real-time measurement of airway deformation with simultaneous measurement of pressure under physiologically relevant static and dynamic conditions- inspiratory peak or peak positive airway pressures of 10-40 cm H_2O, and 20-30 breaths per minute for dynamic studies. We subsequently compare the airway cross sectional areas (CSA) obtained from aOCT and CT, including the change in CSA at different stages of the breathing cycle for dynamic studies, and the CSA at different peak positive airway pressures for static studies. This approach has allowed us to improve our acquisition methodology and to validate aOCT measurements of the dynamic airway for the first time. We believe that this protocol will prove invaluable for aOCT system development and greatly facilitate translation of OCT systems for airway imaging into the clinical setting.

Keywords: dynamic airway imaging, optical coherence tomography, respiratory gated CT, elastography

1. INTRODUCTION

Anatomical Optical Coherence Tomography (aOCT) is a promising modality for airway imaging that can be performed in the physician's office and can yield high resolution, quantitative airway morphology information for improved diagnoses of airway disorders[1]. Several authors have explored the use of OCT for imaging various regions of the airway, both in humans[6, 4, 12] and in animal models[5, 10, 16]. In these studies, aOCT imaging was typically performed under static conditions (for instance at the end of expiration). In such cases, the OCT system was validated against a known phantom and then used to measure tissue morphology or properties within the airway. Studies have also attempted to validate OCT-derived measurements in the airways either qualitatively with images acquired during video endoscopy[17] or quantitatively with histology[13, 5, 16] and with CT scans[14, 15].

However, the *in vivo* mechanical behavior of the airways remains poorly understood and the dynamic changes in the airway geometry during respiration are fundamental to understanding the pathogenesis of obstructive airway disorders such as obstructive sleep apnea syndrome (OSAS)[7]. Significant differences in fluctuations in airway area[8] or the patterns of dynamic airway motion[9] between healthy controls and patients with OSAS have been observed. In addition, assessing airway tissue mechanics *in vivo* could also be important for studying airway remodeling in diseases such as asthma[10, 11]. Fourier Domain OCT, owing to its high temporal and spatial resolution, is ideally suited for dynamic airway imaging. A few studies[10, 11] have performed endoscopic OCT imaging under dynamic conditions, either during tidal breathing or under positive pressure ventilation. In such cases, a simple elastic phantom was typically used for the validation of dynamic OCT imaging or elastography. To the best of our knowledge, dynamic OCT imaging studies of the airways have not been validated against images obtained by another modality within the same specimen under ventilation or tidal breathing.

We have developed an experimental protocol for airway imaging, where both CT and aOCT scans of the airway are performed sequentially during a single exam in a porcine airway model. The setup also includes a ventilator to apply known external positive pressure during imaging and pressure data is acquired synchronously with the OCT data. The protocol is flexible enough to be applied to either *ex vivo* or *in vivo* airway animal studies and can be extended for use in quantitative elastography of the airways. The primary objective of the methods, presented here, is to optimize the aOCT acquisition methodology to improve its accuracy in determining the local airway geometry and elastic properties. Our initial efforts have focused on imaging the trachea due to its relatively simpler geometry and properties as compared to the rest of the airway. We hope to extend the methods developed on the trachea to the more proximal and distal airways in the future.

2. MATERIALS & METHODS

The aOCT system used for the experiments has been previously described[2]. Briefly, it utilizes a wavelength-swept laser source (5 kHz sweep rate, 1310 nm center wavelength, 30 nm sweep range) in a Mach-Zehnder interferometer with a balanced photodetector. The sample arm of the interferometer includes a flexible 170 cm long fiber catheter placed in a protective sheath. The catheter and sheath assembly is 0.86 mm in diameter and is attached at the proximal end to a rotational/ translational stage, which was used to perform rotational scans at 20 Hz with or without simultaneous pull-back at 6 mm/s to scan the specimen under test.

Imaging was performed in the trachea of excised porcine airways or anesthetized live pigs placed on the bed of a Siemens Biograph 64 slice CT system (Siemens Medical Solutions USA Inc.). An endotracheal tube with an inflatable cuff was placed in the airway and a dual swivel adapter was connected to it. The output of a SERVO 900C ventilator (Siemens-Elema AB) was connected to the adapter and used to provide either static continuous positive airway pressures or dynamic pressure controlled ventilation. A flexible 2.5 mm pediatric bronchoscope (11003BC, Karl Storz GmbH & Co.) was introduced into the airway, through the swivel adapter. Video endoscopy was used for real-time guidance of the procedure (see Figure 1(a)). The aOCT catheter was introduced into the trachea through the working channel of the bronchoscope. The pressure signal measured at the inspiratory port of the ventilator was digitized at 1.67 kHz, using the laser sweep trigger as the digitization clock, to provide real-time pressure data during the aOCT scans.

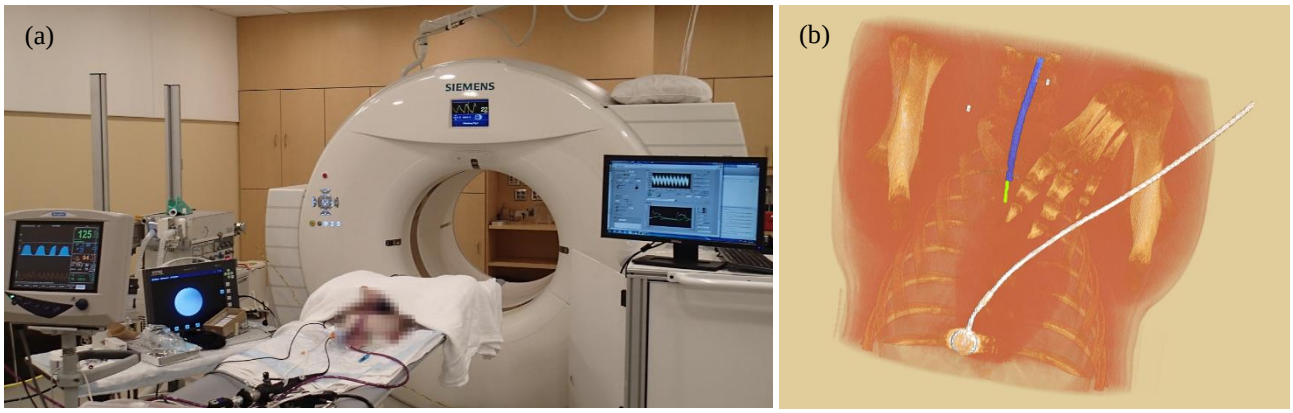

Figure 1: (a) Experimental setup with the live pig: to the left of the CT bed are the vitals monitor, the endoscope video display and the ventilator, the bronchoscope is on the table, the aOCT cart and display are to the right; (b) Volume rendering from a CT scan showing the bronchoscope (blue), the aOCT catheter (yellow) extending from the bronchoscope tip and the respiratory gating sensor (white) attached to the abdomen.

Imaging on the specimens were performed sequentially with aOCT and CT under multiple static inspiratory pressures or dynamic pressure controlled ventilation with multiple peak inspiratory pressures. For static pressure scans, the ventilator maintained 0 (no pressure), 10, 20 or 30 cm H_2O continuous positive airway pressures. At each pressure setting, aOCT and CT scans were performed serially with the bronchoscope at a fixed position. For aOCT imaging, the catheter tip was extended ~28 mm from the bronchoscope tip and a helical pull-back scan was performed, providing 20 frames/s of the target luminal cross-section at a pitch of 0.3 mm. Subsequently, a CT scan with 0.26 mm in-slice pixel spacing and 0.6 mm slice thickness was performed with a field of view large enough to cover the entire airway.

For the dynamic pressure scans, the ventilator was configured to operate in a pressure controlled ventilation mode with the peak inspiratory pressure level of 10, 20, 30 or 40 cm H_2O and at 20 or 30 breaths per minute (bpm). aOCT and CT scans were again performed sequentially at each pressure level with the bronchoscope at a fixed position. The aOCT imaging was performed with similar positioning and rotation rate, but without pull-back. Under dynamic pressures a respiratory gating system (AZ-733V, Anzai Medical Co. Ltd.) was used to acquire CT volumes at specific stages of the respiratory cycle with 0.6 mm pixel spacing and 0.6 mm slice thickness.

The respiratory gating system uses a load cell-based sensor to detect the pig's abdominal motion (see Figure 1(b)) and the abdominal displacement information is processed to determine the respiratory signal, with inspiratory and expiratory phases of the respiratory signal identified using the mean signal level. Each phase was further subdivided into multiple segments with uniform intervals. The CT acquisitions were prospectively triggered at pre-defined segments of the respiratory cycle. In these experiments, CT volumes were acquired at 20% increments of the respiratory signal, yielding 11 volumes (6 volumes during Expiration: Ex100%, Ex80%…Ex0% and 5 volumes during Inspiration: In20%, In40%…In100%) during one respiratory cycle. Respiratory gating for *ex vivo* airways was performed by attaching the respiratory sensor to a bag, which was connected to the ventilation circuit by means of a T-connector. The inflation and deflation of the bag during ventilation served as a surrogate for abdominal motion.

The *ex vivo* porcine airways were suctioned to remove any secretions and the bronchial openings of the tracheas were sutured, to prevent air leakage during the experiments, prior to intubation and imaging. The live animals were anesthetized with Propofol and intubated before the experiments began. The animal's vital signs were monitored throughout the experiment and an appropriate level of anesthesia was maintained by veterinarians and by veterinary technicians. The animal was ventilated with weight appropriate settings prior to and between each data acquisition. The experimental methods used were approved by the Institutional Animal Care and Use Committee at the University of North Carolina, Chapel Hill.

The acquired images were analyzed to determine the Cross Sectional Area (CSA, in mm^2); for analysis of the aOCT images, the luminal surface was segmented using a semi-automated segmentation algorithm similar to our previous method[2, 3], CT images were segmented manually using Mimics (Materialise NV). The position of the aOCT catheter seen on the CT axial images was used to co-register the aOCT and CT images prior to any comparison between them. The cross sectional information derived from the trachea, in combination with pressure, can also be used to infer its elastic properties. In the case of static pressure scans of the *ex vivo* trachea, the intraluminal pressure is the same as the pressure measured at the ventilator and there is no flow. In such cases, the elastic properties of the trachea may be directly computed from the change in cross sectional shape with pressure. However, under dynamic ventilation or for an *in vivo* trachea, the pressure within the trachea is different from the externally applied pressures due to flow and only qualitative information about the tissue elastic properties may be inferred from the change in cross sectional shape and the pressures measured at the ventilator. Importantly, the propensity of a local region of the airway to collapse may be quantified by its compliance[17, 14], one measure of this is the Cross Sectional Compliance[2] (CC, mm^2/cm H_2O), defined as the slope of the CSA-pressure curve ($\Delta CSA/\Delta P$). The local CC was computed along the length of the trachea with the static pressure scans on *ex vivo* tracheae.

3. RESULTS

We performed imaging using the protocol described above on three excised airways and on three live animals. The experimental procedure was refined over these multiple trials. In some of these cases, the imaging parameters were sub-optimal or the results were incorrect due to leaks in the endotracheal cuff or the sutured *ex vivo* airway. This section presents representative results in one live animal and one *ex vivo* trachea.

Under dynamic pressure settings, the aOCT scans were performed without pull-back to acquire images that depict the change in cross sectional shape as a function of time at one position in the trachea. In the case of static pressure scans, the aOCT imaging was performed with pull-back to obtain the cross sectional images of the trachea as a function of distance along the trachea at one positive pressure level. By repeating this procedure at multiple pressures the variation in tracheal shape or volume as a function of pressure was obtained. For both of these cases, the CT scan was performed with a Field of view large enough to cover the whole trachea, which allowed us to determine the cross sectional configuration and size at all points along the trachea.

3.1 *In vivo* trachea results

The variation in CSA under dynamic pressure controlled ventilation in the live animal trachea at a fixed position for aOCT and CT are shown in Figure 2. The ventilator was configured to provide 20 bpm with 1:2 Inspiration: Expiration time ratio and 20 cm H_2O of nominal maximum inspiratory pressure.

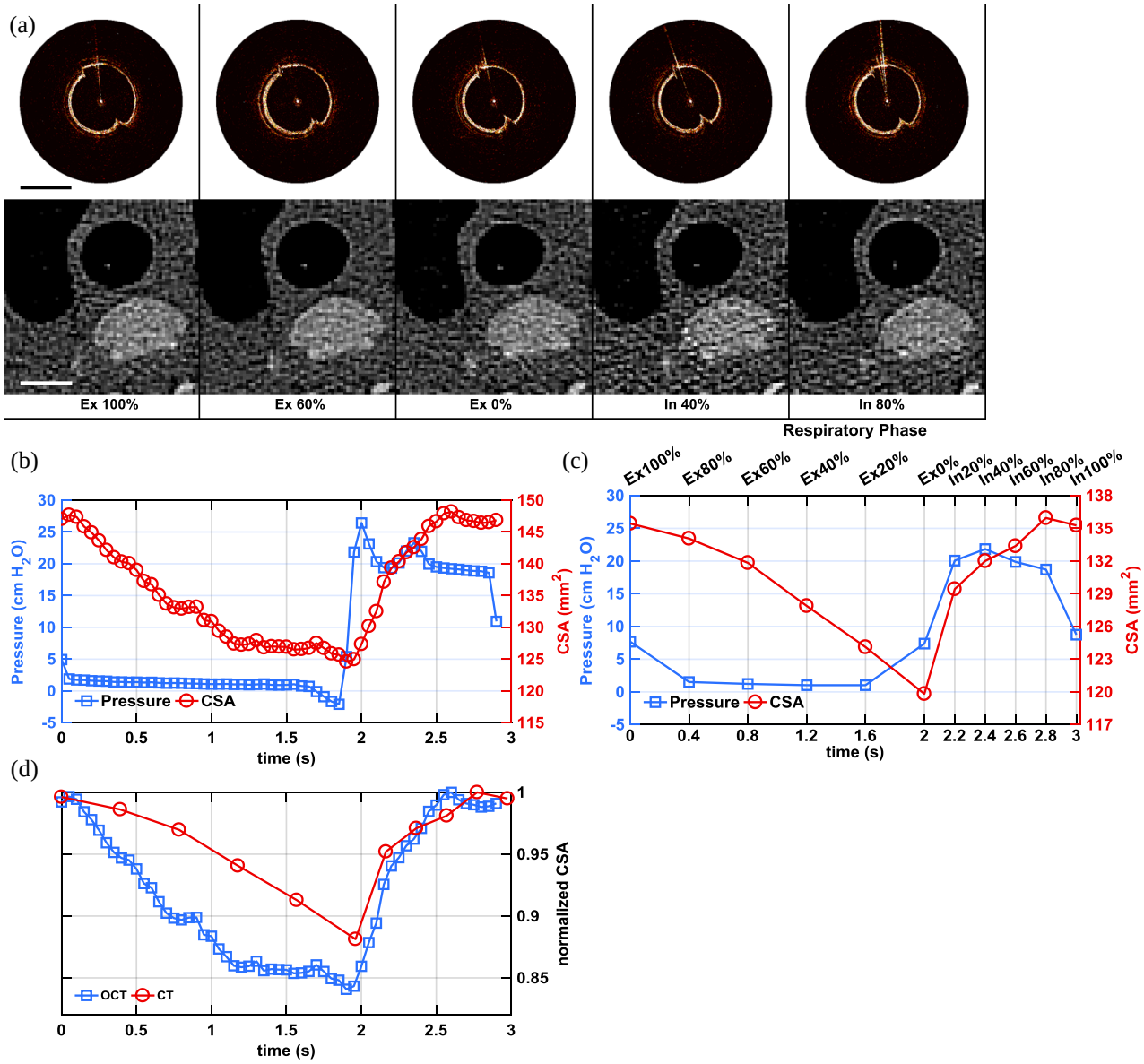

Figure 2: *In vivo* trachea: (a) Cross sectional profile images from OCT (top) and CT (bottom) at different phases of the respiratory cycle, scale bars are 10 mm long; (b) Ventilator output pressure and CSA derived from OCT scans; (c) Ventilator output pressure and CSA derived from CT scans; (d) Comparison between OCT- and CT-derived CSA, normalized

Figure 2(a) shows the images acquired by the aOCT (top) and CT (bottom) systems at different phases of the respiratory cycle. Although difficult to appreciate, both aOCT and CT images indicate a reduction in airway size during expiration and then an increase during inspiration, with the airway size being the smallest at the end expiratory stage of the respiration (denoted as "Ex 0%" in the images); this effect can be quantitatively observed in Figures 2(b) and (c). Figure 2(d) shows

that the change in aOCT CSA measurements over the respiratory cycle correlate well with the CT-derived measurements. The aOCT system acquires 20 cross sectional images per second and therefore acquired 60 measurements over one respiratory cycle; the respiratory gated CT, on the other hand, imaged the trachea at 11 points over the respiratory cycle.

Measurements were repeated, at the same position and with the similar ventilator settings as above, at additional nominal maximum inspiratory pressures of 10, 30 and 40 cm H_2O. Figures 3(a) and (b) show the results of these experiments as measured by aOCT and CT respectively.

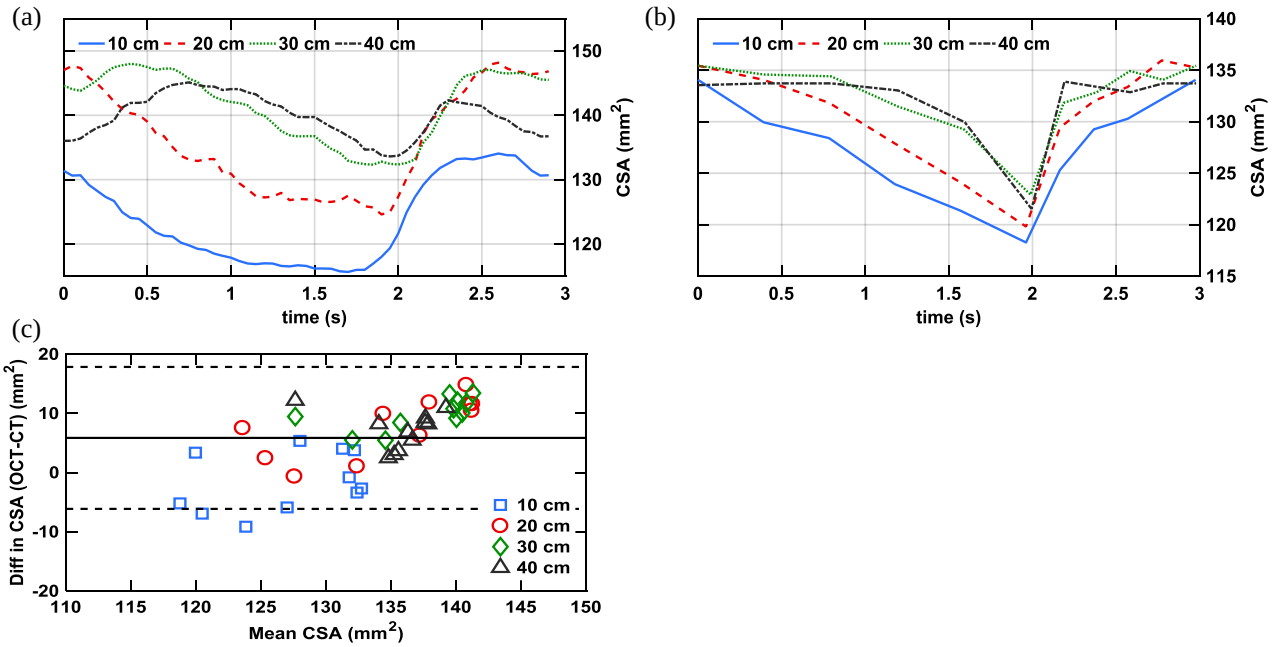

Figure 3: *In vivo* trachea: (a) OCT-derived CSA at a fixed position within the trachea, with pressure controlled ventilation and nominal maximum inspiratory pressures of 10, 20, 30 and 40 cm H_2O; (b) CT-derived CSA under the same settings; (c) Bland-Altman plot of the agreement between measurements of CSA derived from OCT and CT, the solid line represents the mean difference between the two methods (systematic bias), the dashed lines define the limits of agreement (± 2 SD)

The trend in aOCT and CT measured CSA were similar but not identical at the different pressure settings (Figures 3(a) and (b)). The differences in CSA obtained with the two techniques are demonstrated in a Bland-Altman plot (Figure 3(c)), the mean difference between the measurements of CSA was 5.85 mm^2 with limits of agreement (2 SD) from -6.14 to 17.83 mm^2.

3.2 *Ex vivo* trachea results

The variation in CSA under dynamic pressure controlled ventilation in an *ex vivo* trachea at a fixed position for the aOCT and CT scans are shown in Figure 4. The ventilator was programmed to deliver 30 bpm with 1:1 Inspiration: Expiration time ratio and 45 cm H_2O of nominal maximum inspiratory pressure. In his case, the aOCT system produced 40 measurements over a respiratory cycle, whereas, the respiratory gated CT scans produced 11 measurements. The aOCT system was able to follow the ΔCSA over time reasonably well and the trend of increasing CSA with increasing pressure was well depicted (Figure 4(c)) in spite of the differences in the absolute CSA measured (Figure 4(a) and (b)).

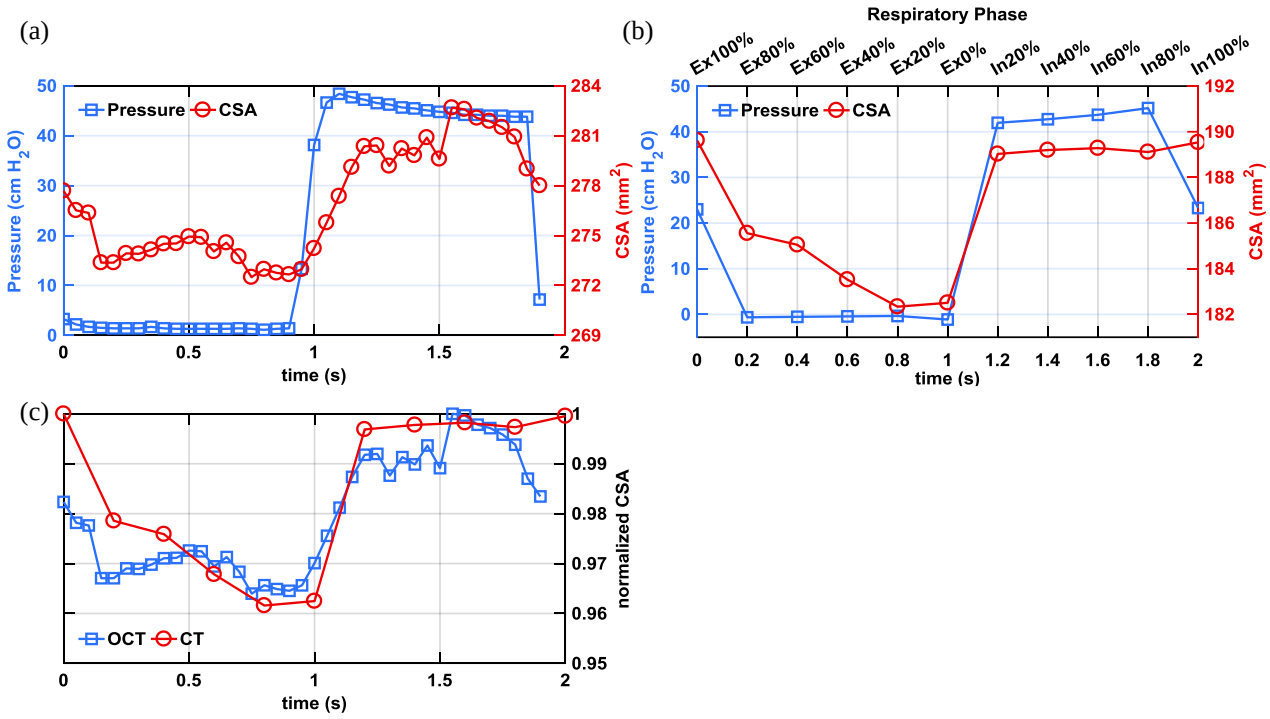

Figure 4: *Ex vivo* trachea: (a) Ventilator output pressure and CSA derived from OCT scans; (b) Ventilator output pressure and CSA derived from CT scans; (c) Comparison between OCT- and CT-derived CSA, normalized

The experimental protocol was also used to compare aOCT and CT-derived measurements of local CC in the same *ex vivo* trachea. The results of the measured CSA and calculated CC by the two methods, under static inspiratory pressures of 0 (no pressure), 10, 20 and 30 cm H_2O are shown in Figure 5. Figure 5(a), (b) depict the variation in CSA measured by aOCT and CT at different positive airway pressures at two positions in the trachea; the slope of the linear regression line is the computed CC. The CSA at 0 cm H_2O was omitted in the CC calculation, as it has been shown[2] that a slight overpressure is needed before the CSA versus pressure curve becomes linear. Figure 5(c) shows the variation in CSA along the entire measured length of the trachea. It can be noted from Figure 5(c) that the CSA measured using both methods increases with increasing pressures and that both modalities indicate that the ΔCSA for pressures increasing from 20 to 30 cm of H_2O was less than the ΔCSA for pressures from 10 to 20 cm H_2O. Figure 5(d) shows the trend in the calculated CC by both methods along the tracheal length.

4. DISCUSSION

This study describes an experimental protocol that enables real-time acquisition of changes in the tracheal geometry with aOCT and CT under externally applied static or dynamic pressures. The acquired images, with both modalities, were subsequently analyzed to determine the airway CSA. The CSA at different peak positive airway pressures and the variation of CSA at different stages of the breathing cycle under various conditions were compared. The trend observed in ΔCSA was roughly similar in both aOCT and CT scans. We observed important differences between *ex vivo* and *in vivo* tracheae when subjected to similar ventilation protocols. The behavior of CSA variation in the *in vivo* trachea, as seen on Figures 3(a) and (b), was remarkable for several reasons: the maximum CSA was the same at all pressure levels and differences in pressures only resulted in differing CSA ranges. It was also interesting to note that the nature of CSA variation with pressure *in vivo* was different from that observed in the *ex vivo* case: Figures 4(a) and (b) are roughly square-wave shaped, while Figures 3(a) and (b) appear saw toothed in shape. This phenomenon is probably attributable to the fact that the soft tissue and skeletal envelope restrict the distension of the trachea in the *in vivo* case; on the other hand, the *ex vivo* trachea has no soft tissue or thorax surrounding it and can therefore distend more. Additionally, the variation of pressure with time at the site of measurement is different in the *in vivo* case, due to the pleural pressure and possibly the action of the airway muscles.

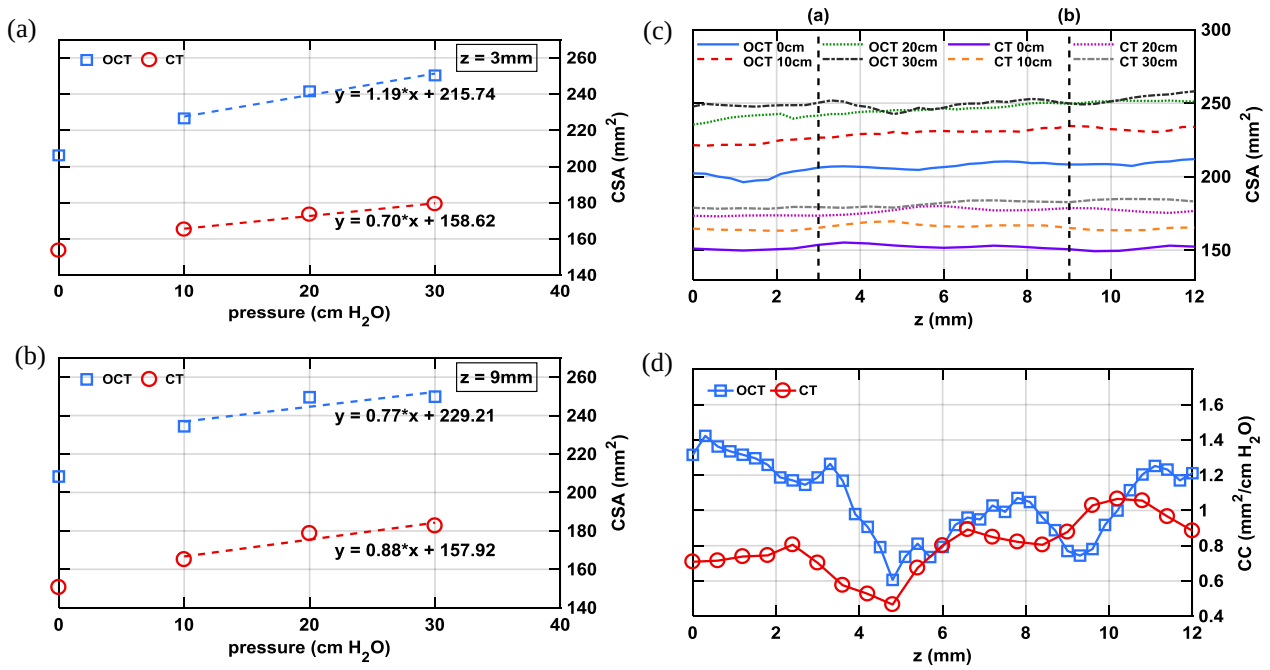

Figure 5: *Ex vivo* trachea: variation in OCT and CT derived CSA as a function of pressure and linear regression fit at (a) position z = 3 mm; (b) position z = 9 mm; (c) OCT and CT derived CSA at all positions along the trachea, with fixed inspiratory pressures of 0 (no pressure), 10, 20 and 30 cm H_2O ; (d) CC as a function of distance along the trachea computed from the CSA values at 10, 20 and 30 cm H_2O; z indicates the position along the trachea

The protocol also enabled us to examine the ΔCSA at different pressure levels in both the *ex vivo* and *in vivo* trachea. In the *in vivo* trachea, the ΔCSA from 30 to 40 cm of H_2O was smaller than that from 20 to 30 cm of H_2O (Figures 3(a) and (b)); similar behavior was also observed in the *ex vivo* case when comparing the ΔCSA from 30 to 20 cm of H_2O to the ΔCSA from 10 to 20 cm of H_2O (Figure 5(c)). The trend of ΔCSA with ΔP has been shown to be linear in our previous *ex vivo* experiments[2] and the non-linearity observed during these experiments could be due to the tracheae reaching their maximal distension at higher pressures. The aOCT- and CT-derived CC along the length of the *ex vivo* trachea were also compared and the observed trends were similar (Figure 5(d)).

The differences in the absolute values of CSA measured by OCT and CT in the *in vivo* trachea was similar to those reported by other studies[14, 3]. However, the aOCT results overestimate the CSA when compared to the CT-derived measurements and in the *ex vivo* case the differences in the measurements by the two methods are significantly larger. The observed differences in the CSA measured with aOCT and CT could be due to a combination of non-uniform rotational distortion (NURD), place-matching errors between the location of the measurements and differences between the planes of data acquisition. NURD is caused by bending of the long catheter that results in variable friction between the rotating catheter and the sheath; under clinical conditions such bends are unavoidable and the non-uniformity of the rotation rate is very difficult to predict or control. The use of catheter tube materials to reduce friction, better torque transmission methods or post-processing algorithms for detecting the rotation rate could help mitigate the effect of such distortions. The contribution of misregistration is not considered to be significant as the catheter tip was used to correlate the CT and aOCT images during our experiments. The aOCT images are acquired without an absolute coordinate system, therefore a tilt in the catheter tip could result in undetected changes in the plane of image acquisition- which in turn would result in differences in CSA measured at a given location within the trachea by the two methods. In our case, since only the trachea was imaged (which has a relatively circular profile), the contribution of this factor to the CSA differences observed is considered to be minimal. Lastly, the lower resolution and limited soft tissue contrast in the CT images compared to aOCT could also lead to differences in CSA measured. However, such factors would probably result in an approximately constant offset between the aOCT and CT measurements on the trachea.

It should be noted that the presented experimental protocol has several important limitations. The endotracheal tube bypasses the upper airway, which is the site for airway collapse in OSAS. The experimental methods presented would have to be modified to use a face-mask instead of an endotracheal tube for upper airway studies or employ a native airway. The ventilation protocol utilizes positive pressure ventilation which is not physiological in nature. Nevertheless, the use of positive pressures allows us to assess the tracheal elastic properties by measuring pressures externally at the ventilator. Additionally, the inspiratory pressure was measured at the ventilator, rather than *in situ*. Both of these limitations can be overcome by the use of a pressure catheter to measure pressures within the trachea at the site of aOCT imaging and subsequently making measurements during spontaneous respiration. The respiratory gated CT acquisitions only acquire 11 samples over the entire respiratory cycle that is 2 or 3 seconds in duration, this may be inadequate to assess any rapid dynamic changes in the airway. While this resolution proved adequate for the comparisons presented here, better assessments could be made by the use of Cine CT acquisition. Finally, CT and aOCT were not acquired simultaneously; however, this should not affect the results presented due to the use of a controlled ventilation setup, respiratory gating, and the close temporal acquisition of the paired data sets.

We believe that the methods described here represent a promising protocol to validate airway OCT measurements under realistic, dynamic conditions. Such validation methods have an important role to play in aOCT system development and will greatly facilitate clinical translation of OCT systems for airway imaging.

5. ACKNOWLEDGMENTS

We would like to thank Mark Hall, Dr. Sorin Mitran, Dr. Julia Kimbell, Matthew Phillips and Amy Davidson for their contributions. This work was funded by the National Institutes of Health, National Heart, Blood, and Lung Institute via grants R01 HL 123557, R21 HL 111968, and R21 HL 130901.

REFERENCES

[1] Chin Loy, A., et al. "Anatomic Optical Coherence Tomography of Upper Airways," Optical Coherence Tomography: Technology and Applications, 2245-2262 (2015)

[2] Bu, R., et al. "Swept-source anatomic optical coherence elastography of porcine trachea," Proceedings of SPIE 9689, 968923 (2016)

[3] Wijesundara, K., et al. "Quantitative upper airway endoscopy with swept-source anatomical optical coherence tomography," Biomedical optics express 5(3), 788-799 (2014)

[4] Walsh, J. H., et al. "Evaluation of pharyngeal shape and size using anatomical optical coherence tomography in individuals with and without obstructive sleep apnoea," Journal of sleep research 17(2), 230-238 (2008)

[5] Lee, A., et al. "Validation of airway wall measurements by optical coherence tomography in porcine airways," PLoS ONE 9(6), e100145 (2014)

[6] McLaughlin, R. A., et al. "Optical coherence tomography in respiratory science and medicine: from airways to alveoli," Physiology 29(5), 369-380 (2014)

[7] Schwab, R. J., et al. "Dynamic upper airway imaging during awake respiration in normal subjects and patients with sleep disordered breathing," American Review of Respiratory Disease 148(5), 1385-1400 (1993)

[8] Arens, R., et al. "Changes in upper airway size during tidal breathing in children with obstructive sleep apnea syndrome," American journal of respiratory and critical care medicine 171(11), 1298-1304 (2005)

[9] Donnelly, L. F., et al. "Upper Airway Motion Depicted at Cine MR Imaging Performed during Sleep: Comparison between Young Patients with and Those without Obstructive Sleep Apnea," Radiology 227(1), 239-245 (2003)

[10] Szabari, M. V., et al. "Using optical coherence tomography (OCT) imaging in the evaluation of airway dynamics (Conference Presentation)," Proceedings of SPIE 9691, 969112 (2016)

[11] Robertson, C., et al. "Investigating in vivo airway wall mechanics during tidal breathing with optical coherence tomography," Journal of biomedical optics 16(10), 106011-106011 (2011)

[12] Volgger, V., et al. "Long-range Fourier domain optical coherence tomography of the pediatric subglottis," International journal of pediatric otorhinolaryngology 79(2), 119-126 (2015)

[13] Hariri, L. P., et al. "Volumetric optical frequency domain imaging of pulmonary pathology with precise correlation to histopathology," CHEST Journal 143(1), 64-74 (2013)

[14] Armstrong, J. J., et al. "Quantitative upper airway imaging with anatomic optical coherence tomography," American journal of respiratory and critical care medicine 173(2), 226-233 (2006)

[15] Williamson, J. P., et al. "Measuring airway dimensions during bronchoscopy using anatomical optical coherence tomography," European Respiratory Journal 35(1), 34-41 (2010)

[16] Lin, J. L., et al. "Real-time subglottic stenosis imaging using optical coherence tomography in the rabbit," JAMA Otolaryngology–Head & Neck Surgery 139(5), 502-509 (2013)

[17] Strohl, K. P., et al. "Mechanical properties of the upper airway," Comprehensive Physiology 2(3), 1853-1872 (2012)